

Imitation from Observations with Trajectory-Level Generative Embeddings

Yongtao Qu*

Shangzhe Li†

Weitong Zhang‡

January 5, 2026

Abstract

We consider the offline imitation learning from observations (LfO) where the expert demonstrations are scarce and the available offline suboptimal data are far from the expert behavior. Many existing distribution-matching approaches struggle in this regime because they impose strict support constraints and rely on brittle one-step models, making it hard to extract useful signal from imperfect data. To tackle this challenge, we propose TGE, a trajectory-level generative embedding for offline LfO that constructs a dense, smooth surrogate reward by estimating expert state density in the latent space of a temporal diffusion model trained on offline trajectory data. By leveraging the smooth geometry of the learned diffusion embedding, TGE captures long-horizon temporal dynamics and effectively bridges the gap between disjoint supports, ensuring a robust learning signal even when offline data is distributionally distinct from the expert. Empirically, the proposed approach consistently matches or outperforms prior offline LfO methods across a range of D4RL locomotion and manipulation benchmarks.

1 Introduction

Imitation learning (IL) has demonstrated remarkable success in enabling agents to acquire complex behaviors across various domains, from robotic manipulation [Florence et al., 2021, Chi et al., 2023, Brohan et al., 2023] to autonomous navigation [Codevilla et al., 2018, Bansal et al., 2019]. By directly supervising state-action mappings, standard IL methods can effectively recover high-performance policies. However, applying these techniques to real-world scenarios poses substantial challenges. A primary bottleneck is the absence of explicit action information in many natural data sources, such as video demonstrations or third-person recordings, which precludes direct supervision of state-action mappings [Torabi et al., 2018, Stadie et al., 2017, Liu et al., 2018]. This has led to the emergence of Learning from Observations (LfO), where the agent must infer desirable behaviors from state-only expert trajectories.

*University of North Carolina at Chapel Hill, Chapel Hill, NC, 27514; email: yongtao@unc.edu

†University of North Carolina at Chapel Hill, Chapel Hill, NC, 27514; email: shangzhe@unc.edu

‡University of North Carolina at Chapel Hill, Chapel Hill, NC, 27514; email: weitongz@unc.edu

While some LfO methods attempt to recover latent actions via inverse dynamics or auxiliary inference mechanisms [Hanna and Stone, 2017, Kidambi et al., 2020], a second, equally critical challenge remains: the quality of available data. In offline settings, the large datasets required for training often contain suboptimal or noisy behaviors arising from human inconsistency, task ambiguity, or domain shifts [Levine et al., 2020, Mandlekar et al., 2022]. Effectively exploiting such imperfect data requires algorithms that can filter noise and extract valuable behavioral priors without being misled by non-expert trajectories.

Despite steady progress, current Learning from Observations (LfO) methods confront structural weaknesses that limit their robustness. Surrogate reward approaches, such as ORIL [Zolna et al., 2020], rely on discriminator or inverse dynamics models to annotate offline data, but their performance can deteriorate over long horizons when the learned signal is imperfect [Ross et al., 2011]. On the other hand, state-of-the-art distribution-matching approaches typically rely on estimating density ratios between expert and offline distributions [Ho and Ermon, 2016, Ma et al., 2022]. However, these methods typically assume the expert behavior is well-covered by the offline data. When distributions are disjoint, strictly aligning them yields sparse or undefined signals, failing to guide the agent towards the expert region. We review these paradigms in more detail in Sec. 2.1.

To address these limitations, we propose **Trajectory-level Generative Embeddings (TGE)**, a novel framework for offline LfO that bypasses the structural reliance on support coverage inherent in density ratio estimation. Instead of relying on brittle density ratios, TGE leverages the smooth, low-dimensional manifold learned by a trajectory-based diffusion model [Janner et al., 2022]. By encoding trajectories into this generative latent space, we construct a dense surrogate reward signal that bridges disjoint supports. We specifically employ a Laplacian kernel with heavy-tailed decay for reward estimation, which ensures an informative reward signal throughout the suboptimal data, preventing the reward collapse issues common in prior distance-based methods. This reward signal effectively guides offline RL algorithms, such as IQIL [Kostrikov et al., 2021] or ReBRAC [Tarasov et al., 2023], toward the expert policy.

Our main contributions are summarized as follows:

- We introduce a trajectory-level representation learning approach based on a generative planner. We find that the resulting latent embeddings are naturally separable and can distinguish between suboptimal and expert-like data in offline datasets, without requiring explicit discriminative training.
- We propose a kernel-based reward formulation defined over the trajectory-level latent embedding, which enables the use of standard offline RL methods for imitation learning with observation-only expert data.
- We empirically evaluate our method across a diverse set of benchmarks. The results show that our approach consistently matches or outperforms state-of-the-art offline learning-from-observations

baselines, with particularly strong robustness in regimes where expert coverage in the offline dataset is limited.

2 Related Work

2.1 Offline Imitation Learning

Offline imitation learning (IL) aims to recover an expert policy from a fixed dataset of demonstrations without access to online environment interactions. While the foundational approach, Behavioral Cloning (BC) [Pomerleau, 1989], treats this as a supervised regression problem, it notoriously suffers from distribution shift and compounding errors when the agent accesses out-of-distribution states [Ross et al., 2011]. To mitigate these compounding errors, distribution-matching approaches shift the objective from local action supervision to global distribution alignment, minimizing the divergence between the learner and expert occupancy measures [Kostrikov et al., 2020, Garg et al., 2021]. Recent advances have largely shifted toward conditional generative modeling to better capture the multimodal nature of the expert’s behavior. Prominent methods now leverage Energy-Based Models [Florence et al., 2021], Transformers [Shafiullah et al., 2022], and Diffusion Models [Chi et al., 2023] to represent complex, non-Gaussian action distributions, thereby enabling robust policy synthesis even in high-dimensional and multimodal settings.

Learning from Observations (LfO) arises as a critical and more challenging subset of this paradigm, where the expert demonstrations lack action labels. Offline LfO approaches generally fall into two distinct paradigms based on how they utilize expert data:

Occupancy Matching This class of methods formulates imitation as a convex optimization problem, solving for the state-occupancy ratio $w(s) = d^{\pi_E}(s)/d^{\pi}(s)$ between the expert and offline data distributions. Methods like SMODICE [Ma et al., 2022] and LobsDICE [Kim et al., 2022] minimizing the KL-divergence between these distributions are often sensitive to the distribution of the offline buffer. Recent variants like PW-DICE [Yan et al., 2024] introduces Wasserstein geometry to relax the strict support constraints, and DILO [Sikchi et al., 2024] utilizes a dual formulation of the χ^2 -divergence to improve stability. Despite these advances, these methods fundamentally rely on estimating density ratios, which can become ill-conditioned when the offline and expert supports are disjoint.

Surrogate Reward Learning Alternatively, two-stage approaches first learn a surrogate reward function $r(s)$ from data and then optimize a policy using offline RL. This paradigm extends beyond imitation learning. It is central to unsupervised reinforcement learning (URLB) [Laskin et al., 2021], where methods typically derive intrinsic pseudo-rewards, such as those based on particle entropy or diversity, to guide policy acquisition in the absence of external supervision. In the context of offline LfO, standard approaches like ORIL [Zolna et al., 2020] employ adversarial learning to train a discriminator-based reward. However, adversarial objectives are notoriously unstable and often produce

signals that are difficult to optimize. TGE falls into this surrogate reward paradigm but circumvents these stability issues by replacing adversarial discriminators with a dense, geometric distance metric derived from latent space of a trajectory-level generative planner trained on the offline dataset.

2.2 Diffusion Models in Reinforcement Learning

Diffusion models have rapidly been adopted in RL, primarily for generative control and data synthesis. In the control domain, diffusion models function as policies [Chi et al., 2024, Wang et al.] or trajectory planners [Janner et al., 2022, Ajay et al., 2022], leveraging iterative denoising to capture multimodal distributions and solve long-horizon tasks. Recent works have extended this to value-based methods, using diffusion to regularize offline Q-learning [Hansen-Estruch et al., 2023]. Beyond control, diffusion models are increasingly used as world models for hallucinating environments [Alonso et al., 2024]. Our work focuses on a distinct application: metric learning. While methods like Stable Rep [Tian et al., 2023] or Diffusion Reward [Huang et al., 2024, Wang et al., 2025] similarly derive learning signals from generative models, they typically rely on static visual semantics from video or image models. In contrast, TGE exploits the trajectory-level latent embedding of a temporal diffusion encoder to capture system dynamics, augmenting the reward-free offline dataset that enables robust imitation without the computational cost of generative sampling during downstream offline RL training.

2.3 Representation Learning in Reinforcement Learning

Representation learning is central to scaling reinforcement learning to high-dimensional observation spaces by extracting compact embeddings that filter task-irrelevant noise. Early approaches largely relied on reconstruction-based auxiliary tasks, utilizing world models or autoencoders to compress sensory inputs into latent states that capture the factors of the environment Ha and Schmidhuber [2018]. To improve robustness to task-irrelevant visual details, subsequent research adopted contrastive learning and bisimulation metrics, which optimize for invariance by grouping states with similar transition dynamics Laskin et al. [2020], Zhang et al. [2020]. However, these approaches typically operate on static state snapshots, which implicitly assumes that single-frame observations are sufficient to distinguish system states. To address this, we depart from single-step encoders and instead employ diffuser Janner et al. [2022] as an encoder to capture trajectory-level representations to provide the temporal context necessary to distinguish behaviors that appear visually identical but possess divergent underlying dynamics.

3 Preliminaries

Markov Decision Process We formulate the learning problem within the standard Markov Decision Process (MDP) framework, defined by the tuple $\mathcal{M} = \langle \mathcal{S}, \mathcal{A}, P, r, \gamma \rangle$, where \mathcal{S} and \mathcal{A} denote the state and action spaces, respectively. The transition kernel $P(s'|s, a)$ specifies the probability of transitioning to a next state s' given the current state s and action a . The reward function $r(s, a)$ provides scalar

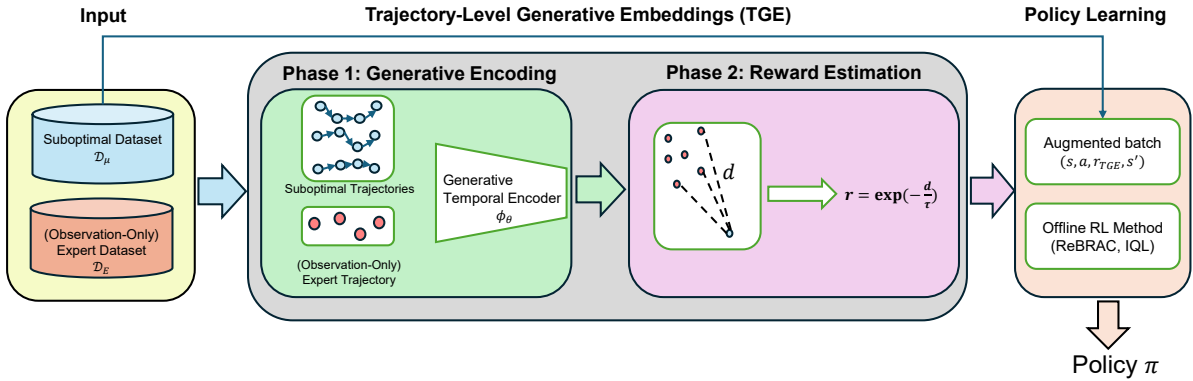


Figure 1: **Overview of Trajectory-level Generative Embeddings (TGE).** The framework employs a trajectory-level diffusion encoder to map trajectory segments into a latent embedding space. A surrogate reward is then computed using a Laplacian kernel over these embeddings to augment the reward-free suboptimal dataset, enabling offline RL training for policy learning.

feedback for each state–action pair, and $\gamma \in [0, 1]$ is a discount factor that determines the weighting of future rewards. A policy $\pi(a|s)$ defines a distribution over actions conditioned on the state, and the objective of reinforcement learning is to identify a policy that maximizes the expected discounted return $J(\pi) = \mathbb{E}_{\pi, P} \left[\sum_{t=0}^{\infty} \gamma^t r(s_t, a_t) \right]$. In imitation learning or learning from observations, both the true reward function r and the expert actions are typically unavailable. Consequently, the learner must infer desirable behaviors from state-only expert trajectories and suboptimal data providing limited state–action coverage.

Offline Imitation Learning from Observations We consider the learning from observation (LfO) setting, where the small expert dataset contains only state observations, without any expert actions or reward annotations. In addition, our work focuses on the offline imitation learning regime, where the agent cannot directly interact with the environment. Instead, we assume access to an offline dataset composed of suboptimal state–action trajectories, which provides the necessary coverage for learning.

Let the expert dataset containing a single expert trajectory be denoted by \mathcal{D}_E , and let \mathcal{D}_μ denote the suboptimal offline dataset consisting of state–action transitions generated by a mixed behavioral policy μ , which contains a combination of expert and suboptimal trajectories. The agent does not have access to the trajectory labels; that is, it cannot directly distinguish which trajectories are expert and which are suboptimal. This setting is standard practice in offline imitation learning from observations [Sikchi et al., 2024, Yan et al., 2024]. We define the normalized discounted state visitation distribution of a policy π as $\rho_\pi(s) = (1 - \gamma) \sum_{t=0}^{\infty} \gamma^t P(s_t = s | \pi)$. Accordingly, let ρ_E , ρ_π , and ρ_μ represent the distributions induced by the expert policy π_E , the learned policy π , and the data-collecting policy μ , respectively. The goal of the learning algorithm is to recover a policy π whose behavior closely matches that of the expert policy π_E .

Denoising Diffusion Probabilistic Models Denoising Diffusion Probabilistic Models (DDPMs) [Ho et al., 2020] are a class of generative models that learn to approximate complex data distributions through a sequence of iterative denoising operations. A DDPM defines a forward diffusion process that gradually corrupts a clean sample $\mathbf{x}_0 \sim q(\mathbf{x}_0)$ by adding Gaussian noise over T time steps according to $q(\mathbf{x}_k \mid \mathbf{x}_{k-1}) = \mathcal{N}(\sqrt{1 - \beta_k} \mathbf{x}_{k-1}, \beta_k I)$, where $\{\beta_k\}_{k=1}^K$ is a variance schedule controlling the noise magnitude at each step. After sufficient diffusion steps, this process yields a nearly isotropic Gaussian distribution $q(\mathbf{x}_K) \approx \mathcal{N}(0, I)$.

The generative (reverse) process is parameterized by a neural network $\epsilon_\theta(\mathbf{x}_k, k)$ that predicts the injected noise and induces the reverse transitions $p_\theta(\mathbf{x}_{k-1} \mid \mathbf{x}_k) = \mathcal{N}(\mu_\theta(\mathbf{x}_k, k), \Sigma_\theta(\mathbf{x}_k, k))$, where the mean $\mu_\theta(\mathbf{x}_k, k)$ is computed from the noise prediction $\epsilon_\theta(\mathbf{x}_k, k)$. Training is performed by minimizing a reweighted variational lower bound, which simplifies to the following mean-squared error objective:

$$\mathcal{L} = \mathbb{E}_{k, \mathbf{x}_0, \epsilon} \left[\left\| \epsilon - \epsilon_\theta(\sqrt{\bar{\alpha}_k} \mathbf{x}_0 + \sqrt{1 - \bar{\alpha}_k} \epsilon, k) \right\|_2^2 \right],$$

where $\bar{\alpha}_k = \prod_{i=1}^k (1 - \beta_i)$. Once trained, the model generates new samples by starting from Gaussian noise $\mathbf{x}_K \sim \mathcal{N}(0, I)$ and iteratively denoising through the learned reverse process. Recent advances in offline reinforcement learning have leveraged diffusion models as trajectory-level generative planners, enabling long-horizon reasoning and multi-modal trajectory generation [Janner et al., 2022, Ajay et al., 2022].

4 Methodology

We aim to develop a novel offline imitation learning from observations framework that leverages trajectory-level generative planners as encoders. Such planners enable the algorithm to reason over extended horizons and incorporate rich temporal structure that is difficult to capture using stepwise imitation approaches. To achieve this, we propose **Trajectory-level Generative Embeddings** (TGE), a method that constructs reward signals from the latent embeddings of a generative planner trained to perform density estimation over both the suboptimal dataset \mathcal{D}_μ . These trajectory-level latent embeddings provide a discriminative representation capable of distinguishing expert-like and suboptimal trajectories, thereby serving as an informative reward proxy for offline policy optimization on \mathcal{D}_μ . Finally, we train an offline RL algorithm on the suboptimal dataset using the TGE-derived reward function. The overall procedure is summarized in Algorithm 1, and an overview of the pipeline is illustrated in Figure 1.

4.1 Generative Planner Learns Separable Embeddings

Recent work has shown that diffusion models can be viewed through the lens of denoising autoencoders across multiple noise scales, and that intermediate diffusion features can serve as useful representations for downstream tasks Fuest et al. [2024]. In particular, Yang and Wang [2023] propose to extract and distill multi-timestep diffusion representations (RepFusion) and demonstrate strong performance on

recognition benchmarks, suggesting that diffusion training induces semantically meaningful feature hierarchies.

Motivated by this perspective, we treat the encoder of the trajectory diffusion planner Diffuser Janner et al. [2022] as an unsupervised representation learner and use its trajectory-level latent embedding for imitation. Specifically, as outlined in Line 1 of Algorithm 1, we train the diffusion noise model on the suboptimal dataset \mathcal{D}_μ using the objective

$$\mathcal{L}(\theta) = \mathbb{E}_{\tau_0 \sim \mathcal{D}_\mu, k, \epsilon} [\|\epsilon - \epsilon_\theta(\tau_k, k)\|_2^2], \quad (1)$$

where $k \sim \text{Unif}[K]$ denotes the diffusion timestep, $\epsilon \sim \mathcal{N}(0, I)$ is the Gaussian noise target, and τ_k is the noised trajectory obtained by adding noise to the clean trajectory τ_0 with length H at diffusion timestep k . Let $\tau \in \mathcal{T}$ denote a state-action trajectory of length H , where the trajectory space is defined as $\mathcal{T} = \mathbb{R}^{H \times (|\mathcal{S}|+|\mathcal{A}|)}$. The noise model ϵ_θ is parameterized using a U-Net architecture [Ronneberger et al., 2015], which we conceptually decompose into a temporal encoder $\phi : \mathcal{T} \times \mathbb{R} \rightarrow \mathcal{Z}$ and a decoder $\psi : \mathcal{Z} \times \mathbb{R} \rightarrow \mathcal{T}$, such that $\epsilon_\theta(\tau_k, k) = (\phi_\theta \circ \psi_\theta)(\tau_k, k)$. Minimizing the denoising score-matching objective in Equation (1) encourages the latent representation \mathcal{Z} to preserve information about the underlying clean trajectory distribution, as it must support reconstruction across a range of Gaussian noise levels. Consequently, \mathcal{Z} captures temporally coherent features that are stable under perturbations, yielding an embedding space that is more semantically discriminative for downstream similarity-based rewards.

Given a clean input trajectory $\tau_0 \sim \mathcal{D}_\mu$, we extract a latent embedding using only the encoder. Figure 2 illustrates that, even without any explicit discriminative supervision between expert-like and suboptimal trajectories in \mathcal{D}_μ , the encoder-induced embedding $z = \phi_\theta(\tau_0, 0)$ naturally separates expert-like samples from suboptimal ones in the mixed dataset. Given this desirable separation property of the embeddings, it is natural to leverage them for reward construction by directly measuring an appropriate distance between embeddings.

4.2 Reward Estimation on Trajectory-level Embeddings

We now describe the procedure for generating synthetic rewards based on the trajectory-level embeddings induced by the encoder of the generative planner. Given the expert dataset \mathcal{D}_E , we first extract a set of expert embeddings $\mathcal{Z}_E = \{z_E = \phi_\theta(\tau) \mid \tau \in \mathcal{D}_E\}$ from the state-only expert trajectories (Line 2 in Algorithm 1). For each state s_t in the suboptimal dataset \mathcal{D}_μ , we consider the trajectory segment that follows it, $\tau_\mu = s_{t:t+H}$, and encode it into a latent vector $z_t = \phi_\theta(\tau_\mu)$. In the expert embedding space \mathcal{Z}_E , we compute the L_2 -norms between z_t and all expert embeddings $z_E \in \mathcal{Z}_E$, and then identify the top- m nearest neighbors, denoted by $\mathcal{N}_m(\mathcal{Z}_E)$. This nearest-neighbor retrieval serves as a proxy for density estimation; we provide the theoretical derivation linking this metric to particle-based entropy maximization Liu and Abbeel [2021] in Section 4.3.

To estimate how likely a suboptimal trajectory segment τ_μ resembles an expert trajectory, we apply

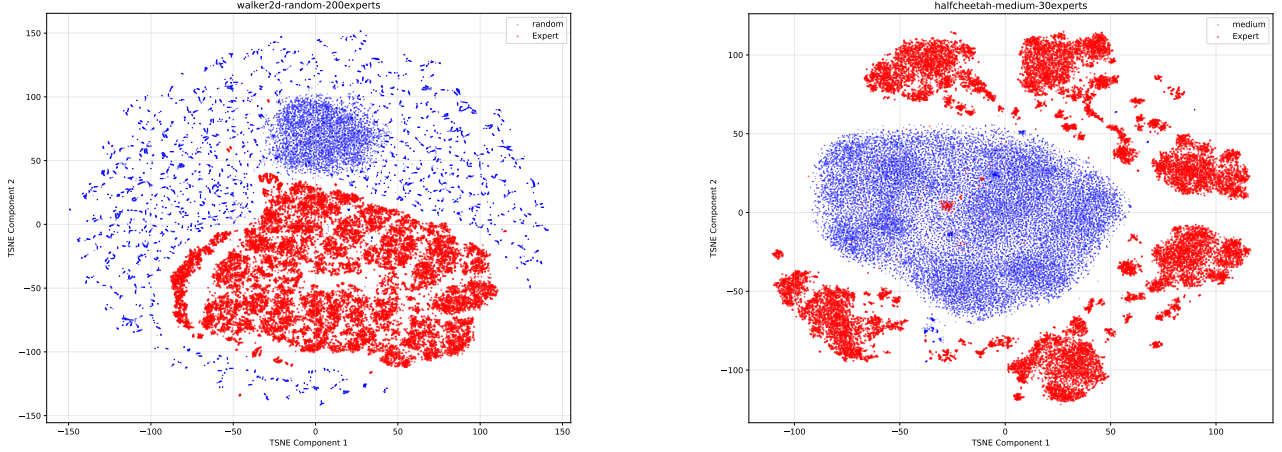


Figure 2: **T-SNE Embedding Visualization.** The latent embeddings produced by the generative planner naturally separate expert transitions from suboptimal ones. As shown, expert samples (colored in red) and suboptimal samples (colored in blue) form distinct clusters with a clear boundary, indicating that the trajectory-level embedding space is highly discriminative.

a Parzen–Rosenblatt estimator on the distances between z_t and its m nearest expert neighbors:

$$r_{\text{TGE}}(s_t) = \frac{1}{m} \sum_{z_E \in \mathcal{N}_m(\mathcal{Z}_E)} f(\|z_t - z_E\|_2 / \sigma), \quad (2)$$

where σ is a kernel temperature. Note that we normalize all latent embeddings by projecting them onto the unit sphere (dividing each vector by its L_2 -norm), ensuring that all embeddings have equal length and allowing for consistent distance computations under the kernel. We adopt a Laplacian kernel $f(d) = \exp(-d)$ rather than the standard Gaussian kernel, as we observe empirically that Gaussian kernels $\exp(-d^2)$ decay too aggressively in high-dimensional latent spaces, resulting in overly sparse rewards on suboptimal data. In contrast, the heavier tail of the Laplacian kernel provides denser gradients that more effectively guide the agent from suboptimal regions toward the expert subspace.

4.3 Downstream Policy Learning

Since the original suboptimal dataset \mathcal{D}_μ consists of state–action transitions without reward labels, the reward estimation procedure described in Section 4.2 enables us to annotate each transition with a synthetic reward $r_{\text{TGE}}(s)$, which measures the similarity of the current state to the expert state distribution. Higher values indicate stronger expert-likeness, while lower values correspond to more suboptimal behavior.

With these synthetic rewards, the augmented dataset $\mathcal{D}'_\mu = \{(s_t, a_t, r_{\text{TGE}}(s_t))\}$ can be used to train any offline RL method for policy learning. In our experiments, we adopt two state-of-the-art offline RL algorithms, Implicit Q-Learning (IQL) [Kostrikov et al., 2021] and Revisited Behavior Regularized Actor-Critic (ReBRAC) [Tarasov et al., 2023], and demonstrate that both methods effectively learn high-quality policies when equipped with our synthetic reward signal.

Algorithm 1 Trajectory-Level Generative Embeddings

Require: Offline suboptimal dataset \mathcal{D}_μ , expert dataset \mathcal{D}_E , horizon H , number of candidates m , temperature σ , and a kernel function $f(\cdot)$.

- 1: Train generative planner on \mathcal{D}_μ and extract the encoder ϕ_θ .
- 2: Compute embeddings $\mathcal{Z}_\mu = \phi_\theta(\mathcal{D}_\mu)$ and $\mathcal{Z}_E = \phi_\theta(\mathcal{D}_E)$ on trajectory segments length H .
- 3: Project all latent vectors to a unit sphere: $z \leftarrow z/\|z\|_2$.
- 4: **for** each $z_t \in \mathcal{Z}_\mu$ **do**
- 5: Compute distances $d(z_t, z_E) = \|z_t - z_E\|_2$ for all $z_E \in \mathcal{Z}_E$.
- 6: Construct the top- m nearest neighbor $\mathcal{N}_m(\mathcal{Z}_E)$.
- 7: $r_{\text{TGE}}(s_t) \leftarrow \frac{1}{m} \sum_{j \in \mathcal{N}_m(\mathcal{Z}_E)} f(-d(z_t, z_E)/\sigma)$.
- 8: **end for**
- 9: Run any offline RL algorithm on the suboptimal dataset augmented with the synthetic rewards, i.e., $\mathcal{D}'_\mu = \{(s_t, a_t, r_{\text{TGE}}(s_t))\}$.

4.4 Reward Interpretation and Learning Signals

An Entropy Perspective on the Reward Formulation It is important to note that conducting policy learning by maximizing the reward defined in Eq. 2 is equivalent to minimizing an approximation of the particle-based cross-entropy between the latent expert distribution and the behavioral distribution. Specifically, given n data points $\{z_i\}_{i=1}^n$ sampled from a latent state distribution induced by a policy π , we leverage non-parametric entropy estimation techniques Singh et al. [2003], Liu and Abbeel [2021] to express the particle-based cross-entropy with respect to the expert distribution as:

$$H(\rho_\pi, \rho_E) = -\frac{1}{n} \sum_{i=1}^n \log \left(\frac{m}{nv_i^m} \right) + b(m) \propto \sum_{i=1}^n \log v_i^m,$$

where $b(m)$ is a bias correction term depending solely on the nearest neighbor parameter m . Here, v_i^m denotes the volume of a hypersphere with radius $\|z_i - z_E^m\|$, representing the Euclidean distance between a policy datapoint z_i and its m -th nearest neighbor in the expert distribution:

$$v_i^m = \frac{\pi^{d_z/2}}{\Gamma(d_z/2 + 1)} \|z_i - z_E^m\|^{d_z},$$

where $d_z = |\mathcal{Z}|$ is the dimension of the latent space and Γ is the gamma function. Consequently, by substituting the volume term, the cross-entropy can be reformulated as:

$$H(\rho_\pi, \rho_E) \propto \sum_{i=1}^n \log \|z_i - z_E^m\|^{d_z}.$$

This entropy estimator indicates that minimizing cross-entropy requires minimizing the distances between the agent's states and their expert neighbors. Given that the reward function we applied $f(d) = e^{-d} \approx 1 - \log(1 + d)$, optimizing the policy to maximize the reward in Eq. 2 is similar with minimizing the cross-entropy between the latent distributions of the expert and behavioral policies.

Analysis of Learning Signals Building on the entropy-based interpretation of our reward, we analyze the structural differences between our generative metric learning approach and the prevailing distribution-matching paradigm.

Dual optimization methods fundamentally rely on estimating density ratios, $w(s) \approx d^{\pi_E}(s)/d^{\mathcal{D}_\mu}(s)$, to reweight offline transitions. This formulation typically assumes a nontrivial degree of support overlap Ma et al. [2022], such that expert transitions are reasonably represented within the offline dataset. In more realistic settings where the offline data is largely disjoint from the expert distribution, this ratio can become ill-conditioned. For suboptimal states outside the expert support, $d^{\pi_E}(s) \rightarrow 0$, causing importance weights to vanish. As a result, supervision concentrates on a small subset of in-support states, while much of the offline data receives nearly indistinguishable near-zero weights, limiting the ability to provide graded feedback on how different suboptimal behaviors compare or how they should be improved.

In contrast, TGE reduces its reliance on strict support overlap by constructing a distance-shaped reward in a learned latent space. Rather than assigning near-uniformly negligible supervision to out-of-distribution states, the exponential kernel $r(s) \propto \exp(-d(z_s, z_E)/\tau)$ induces a smoothly decaying, graded signal as a function of distance. This allows many suboptimal trajectories to remain comparable through their relative proximity to expert behavior, providing a usable preference signal that prioritizes trajectories closer to the expert instead of restricting learning to a small overlapping subset.

The effectiveness of this extrapolation depends on the semantic quality of the underlying metric. Standard distance metrics, such as L_2 distance on raw observations, often fail due to state aliasing, where states that are close under a raw metric may be functionally distinct (e.g., spatially proximate states separated by an obstacle in maze environments). By leveraging the encoder of a trajectory-level diffusion model, ϕ_θ , we exploit the model’s generative inductive bias, which is trained to capture joint temporal structure over trajectories. As a result, the induced latent space is organized according to long-horizon dynamics rather than superficial static features, making the resulting distances more reflective of functional similarity and better suited for robust imitation learning.

5 Experiments

5.1 Experimental Setup

Environments and Datasets We evaluate our method on offline learning-from-observations (LfO) benchmarks built on D4RL, covering both locomotion and manipulation domains. The locomotion tasks are based on MuJoCo, including `hopper`, `halfcheetah`, `walker2d`, and `ant`, while the manipulation tasks are based on Adroit, including `pen`, `door`, and `hammer`. For MuJoCo, the offline suboptimal dataset \mathcal{D}_μ contains approximately 1M transitions drawn from the D4RL `random` or `medium` datasets, following established LfO protocols used in SMODICE [Sikchi et al., 2024] and DILO [Yan et al., 2024]. For Adroit, \mathcal{D}_μ consists of `human` and `cloned` trajectories, again adhering to the standard benchmark protocol.

Following prior work, we consider two mixture settings that differ in the proportion of expert transitions included in \mathcal{D}_μ : (i) *expert*, in which \mathcal{D}_μ contains 200 expert trajectories, and (ii) *few-expert*, in which \mathcal{D}_μ contains 30 expert trajectories. For the detailed mixture strategy, we refer to Appendix B.

Expert data All methods are additionally provided with an **observation-only** demonstration \mathcal{D}_E consisting of a single expert trajectory, which supplies the expert state sequence required by learning-from-observations (LfO) algorithms.

Baselines and Evaluation We compare against recent offline learning-from-observations (LfO) methods, including SMODICE Ma et al. [2022], PW-DICE Yan et al. [2024], and DILO Sikchi et al. [2024], which have been shown to outperform earlier approaches such as LobsDICE Kim et al. [2022] and DemoDICE Kim et al. [2021]. We additionally include trajectory-level behavior cloning (BC) as a baseline, trained on the suboptimal data using a diffuser [Janner et al., 2022] without reward guidance. Each configuration is evaluated with three random seeds, and we report the mean and standard deviation of normalized D4RL scores across seeds for all tasks and methods. We provide implementation details and hyperparameter settings in Appendix A, along with detailed training dynamics visualizations in Appendix D.

5.2 Experimental Results

Performance on MuJoCo Locomotion Benchmarks As shown in Table 1, TGE combined with existing offline RL backbones consistently matches or outperforms all baselines. The performance gains are most pronounced in the `medium+few-expert` and `medium` regimes across all environments (`hopper`, `halfcheetah`, `walker2d`, and `ant`).

In these settings, where the offline dataset contains limited expert-level data, occupancy-matching methods such as DILO [Sikchi et al., 2024] and PW-DICE [Yan et al., 2024] suffer substantial performance degradation and often fail to recover a functional policy. In contrast, TGE-based reward estimation, when combined with standard offline RL backbones, maintains robust performance across these regimes, resulting in a clear margin over prior approaches. These empirical findings support our analysis in Section 4.4, which suggests that occupancy-matching objectives become less informative under severe support mismatch between \mathcal{D}_μ and \mathcal{D}_E . By constructing rewards based on geometric proximity in the latent space of the generative planner, rather than direct support overlap, TGE is able to recover meaningful reward signals even when the support mismatch is large, thereby bridging the gap where occupancy ratio-based methods tend to fail.

Performance on Adroit Manipulation Benchmarks In the high-dimensional Adroit domain of dexterous hand manipulation, we observe a trade-off between handling human-collected and generated data. When combined with downstream offline RL backbones, TGE-based reward estimation performs particularly well on the `human+expert` datasets, establishing a new state of the art by consistently

Table 1: **Main Results.** TGE (combined with IQL or ReBRAC, highlighted in **cyan**) is compared against state-of-the-art offline LfO baselines. The results demonstrate that TGE achieves superior performance. We report the mean and standard deviation for each result with 3 random seeds. Results that show statistically significant improvements over the second-best method (t-test) are highlighted in **bold**.

Dataset	Env	Diffuser (BC)	SMODICE	PW-DICE	DILO	TGE+IQL	TGE+ReBRAC	Expert
random+expert	hopper	1.45±0.17	103.79±4.76	106.22±8.21	104.96±6.52	110.71±0.40	110.08±1.51	111.34
	halfcheetah	0.15±0.49	77.10±6.72	90.63±1.08	89.40±2.65	88.70±1.32	92.52±0.67	88.83
	walker2d	-0.01±0.04	108.74±0.72	107.97±0.94	108.88±0.39	108.39±0.53	107.58±0.56	106.93
	ant	9.58±4.77	124.10±2.19	123.15±8.48	122.87±4.18	122.58±4.04	122.91±8.74	130.75
random+few-expert	hopper	1.38±0.06	62.04±17.02	89.32±17.29	92.66±7.42	84.07±8.55	89.43±13.81	111.34
	halfcheetah	0.03±0.54	2.60±0.64	31.16±32.38	48.26±14.18	5.76±1.98	47.99±7.77	88.83
	walker2d	0.01±0.03	16.97±35.72	97.68±10.98	107.32±1.96	40.59±5.85	106.83±0.82	106.93
	ant	7.25±0.07	32.11±8.38	108.08±15.99	112.50±7.77	32.21±3.66	112.46±5.30	130.75
medium+expert	hopper	45.52±4.81	57.77±8.32	69.38±28.15	102.52±5.73	81.10±24.27	109.19±0.41	111.34
	halfcheetah	41.33±0.49	57.27±2.20	60.76±3.15	89.98±0.61	85.21±1.02	89.35±0.60	88.93
	walker2d	59.74±5.69	70.03±18.38	85.17±6.85	108.52±0.71	104.40±4.45	109.19±1.04	106.93
	ant	87.42±6.38	104.68±5.21	117.51±6.84	92.41±2.62	108.40±2.69	125.18±0.95	130.75
medium+few-expert	hopper	50.74±2.92	52.02±2.64	56.79±11.55	38.07±11.56	73.83±2.35	97.24±2.22	111.34
	halfcheetah	41.49±1.28	41.60±2.99	46.33±7.44	66.07±8.52	55.71±1.36	86.42±2.80	88.83
	walker2d	61.57±6.92	73.72±4.57	80.77±3.14	70.19±2.51	78.12±1.85	105.79±2.07	106.93
	ant	86.13±7.24	89.11±1.53	101.26±8.73	92.55±5.60	95.95±3.13	122.76±0.39	130.75
medium	hopper	46.33±1.86	56.18±1.16	65.82±11.39	48.68±17.85	67.67±4.19	63.99±1.41	111.34
	halfcheetah	41.64±0.30	42.44±0.50	43.27±0.58	42.07±0.47	44.93±0.13	46.63±0.60	88.83
	walker2d	65.62±4.89	71.28±7.21	75.64±3.58	69.74±1.13	75.81±4.26	82.10±1.42	106.93
	ant	85.67±11.66	88.94±2.89	94.90±4.55	90.13±4.68	89.93±2.28	114.40±1.05	130.75
cloned+expert	pen	30.98±46.56	22.63±6.35	1.49±3.61	61.05±10.86	58.95±4.14	63.15±5.11	167.18
	door	0.27±1.84	-0.08±0.08	1.17±2.16	100.90±2.48	0.02±0.00	1.23±2.07	103.95
	hammer	0.59±0.19	0.48±0.46	6.00±5.44	54.29±23.25	1.34±1.06	37.84±8.05	125.72
human+expert	pen	73.84±18.47	47.64±14.83	27.71±6.32	99.33±10.13	105.61±9.33	90.30±5.36	167.18
	door	47.21±12.72	1.50±1.06	0.06±0.03	96.45±4.55	101.49±3.87	101.43±3.73	104.73
	hammer	42.33±20.70	0.34±0.23	29.26±34.09	91.24±13.50	118.43±6.97	109.63±9.16	125.72

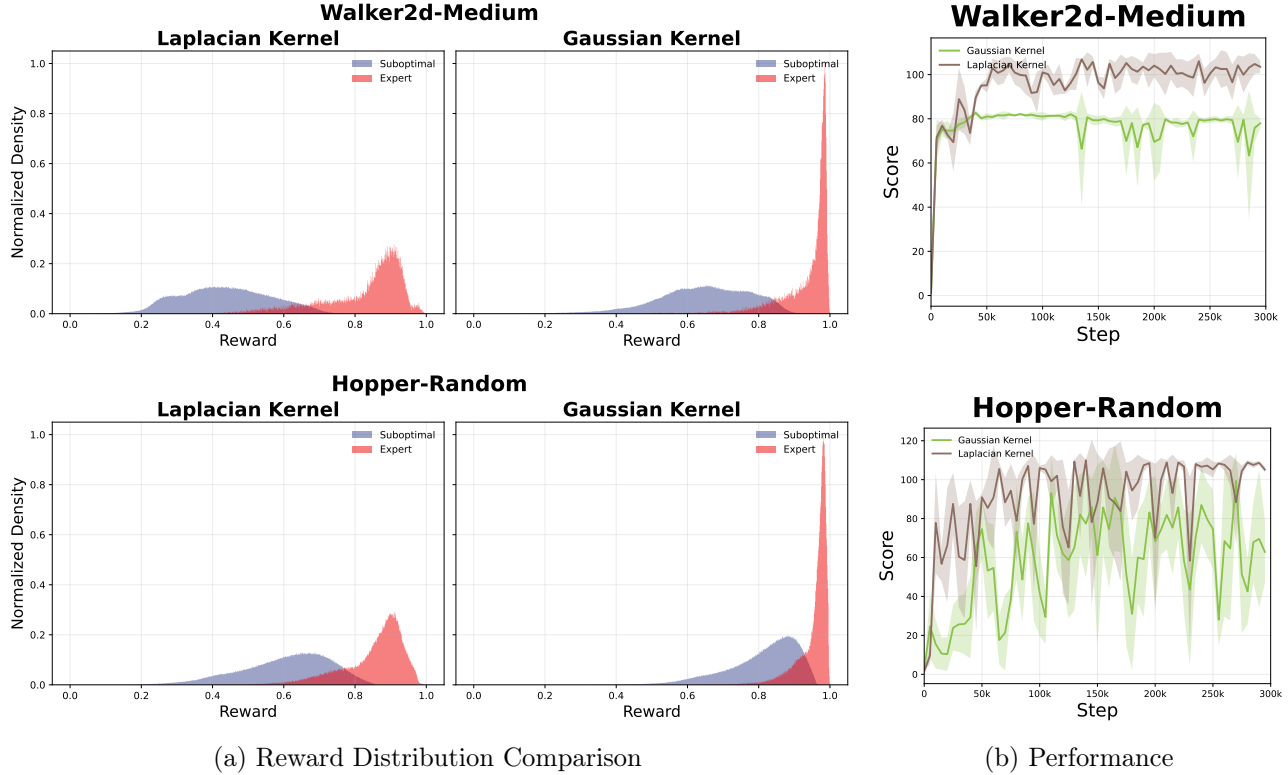


Figure 3: **Ablation of the Reward Signal Density.** (Top) Walker2d-Medium. (Bottom) Hopper-Random. Distributions of synthetic rewards assigned to expert (red) and suboptimal (blue) data. Compared to Gaussian-kernel-based reward estimation, the Laplacian kernel preserves a heavier-tailed reward signal and is associated with improved performance and training stability.

outperforming DILO [Sikchi et al., 2024] and PW-DICE [Yan et al., 2024] across all tasks. These results highlight the robustness of TGE to diverse and potentially non-Markovian noise present in human demonstrations.

On the `cloned+expert` datasets, performance is more mixed. While TGE achieves the highest score on `pen`, it underperforms DILO on `door` and `hammer`. A possible explanation is that cloned data is generated by a relatively consistent policy, under which density-ratio-based methods such as DILO may be better able to exploit the resulting structural overlap between expert and generated data distributions.

Nevertheless, the strong performance of TGE-based method on human data underscores its practical relevance for real-world settings, where data collection is often noisy and less structured.

5.3 Ablation Studies

Choice of Kernels for Reward Estimation We investigate the choice of kernel function by analyzing the resulting reward distributions and their associated training dynamics. Figure 3(a)

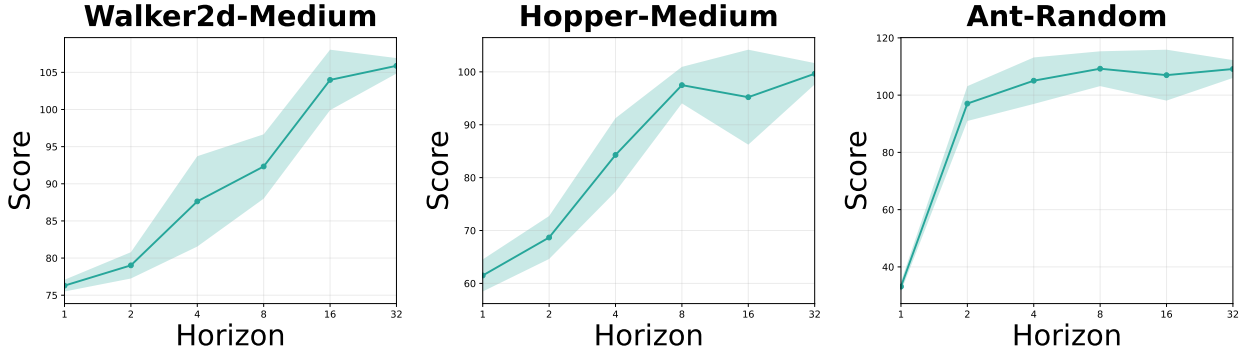


Figure 4: **Ablation of the Temporal Horizon.** The results demonstrate how performance varies with the context horizon H . We observe that larger H generally leads to improved performance, highlighting the importance of temporal context.

visualizes the density of synthetic rewards assigned to expert and suboptimal trajectories in the offline dataset under Laplacian and Gaussian kernels, respectively.

As shown in Figure 3(a, right), the Gaussian kernel produces a reward distribution that is highly concentrated in narrow regions: expert rewards collapse near 1.0, forming a sharp peak, while suboptimal trajectories cluster nearby. As a result, meaningful behavioral differences correspond to only minor reward variations, which limits the clarity of the learning signal. In contrast, the Laplacian kernel (Figure 3(a, left)) yields a broader, heavy-tailed reward distribution. Its linear log-decay better preserves the relative ordering of trajectories in the embedding space, improving reward separability. This enhanced distinguishability facilitates more accurate value estimation by the critic and leads to more stable and optimal learning curves, as shown in Figure 3(b).

Impact of Horizons in the Generative Planner We further examine how the length of temporal context used by the generative planner influences reward estimation quality and, in turn, the performance of the downstream offline RL policy. Specifically, we vary the horizon length H employed during planner training and embedding computation. As shown in Figure 4, using a single-step encoding ($H=1$) leads to a substantial degradation in the final policy performance, highlighting the importance of incorporating temporal context along the trajectory. Increasing H yields nearly consistent performance improvements across tasks, with gains saturating around $H=32$. This trend suggests that short-to-mid temporal windows are sufficient to capture essential dynamic information, while longer horizons provide diminishing returns and may introduce unnecessary computation or over-smoothing effects. Based on these observations, we adopt $H=32$ as the default setting, which provides a strong and stable trade-off across environments.

We provide additional ablation studies on the kernel temperature and the number of nearest neighbors in Appendix C.

6 Conclusion

In this work, we introduced Trajectory-level Generative Embeddings (TGE), a novel framework for offline imitation learning from observations that addresses the structural limitations of distribution-matching approaches. By shifting the paradigm from density ratio estimation to generative metric learning, TGE overcomes the support coverage assumption that hampers prior methods. We demonstrated that encoding trajectories into the latent manifold of a temporal diffusion model allows for the construction of a dense, informative reward signal even when the offline data is distributionally disjoint from the expert.

These findings suggest that generative models can serve as powerful tools for structuring the state space in reinforcement learning, going beyond their traditional roles in planning and synthesis. Future work could explore extending this manifold-based reward framework to online fine-tuning settings or leveraging larger-scale video diffusion models to enable imitation from cross-embodiment observations.

References

- Anurag Ajay, Yilun Du, Abhi Gupta, Joshua Tenenbaum, Tommi Jaakkola, and Pulkit Agrawal. Is conditional generative modeling all you need for decision-making? *arXiv preprint arXiv:2211.15657*, 2022.
- Eloi Alonso, Adam Jolley, Vincent Micheli, Anssi Kanervisto, Amos J Storkey, Tim Pearce, and François Fleuret. Diffusion for world modeling: Visual details matter in atari. *Advances in Neural Information Processing Systems*, 37:58757–58791, 2024.
- Mayank Bansal, Alex Krizhevsky, and Abhijit Ogale. Chauffeurnet: Learning to drive by imitating the best and synthesizing the worst. In *Robotics: Science and Systems (RSS)*, 2019.
- Anthony Brohan, Noah Brown, Justice Carbalal, Yevgen Chebotar, Joseph Dabis, Chelsea Finn, Keerthana Gopalakrishnan, Karol Hausman, Alexander Herzog, Jasmine Hsu, et al. Rt-1: Robotics transformer for real-world control at scale. In *Robotics: Science and Systems (RSS)*, 2023.
- Cheng Chi, Siyuan Feng, Yilun Du, Zhenjia Xu, Eric Cousineau, Benjamin Burchfiel, and Shuran Song. Diffusion policy: Visuomotor policy learning via action diffusion. In *Robotics: Science and Systems (RSS)*, 2023.
- Cheng Chi, Zhenjia Xu, Siyuan Feng, Eric Cousineau, Yilun Du, Benjamin Burchfiel, Russ Tedrake, and Shuran Song. Diffusion policy: Visuomotor policy learning via action diffusion. *The International Journal of Robotics Research*, 2024.
- Felipe Codevilla, Matthias Müller, Antonio López, Vladlen Koltun, and Alexey Dosovitskiy. End-to-end driving via conditional imitation learning. In *2018 IEEE international conference on robotics and automation (ICRA)*, pages 4693–4700. IEEE, 2018.

Pete Florence, Corey Lynch, Andy Zeng, Oscar Ramirez, Ayzaan Wahid, Laura Downs, Adrian Wong, Johnny Lee, Igor Mordatch, and Jonathan Tompson. Implicit behavioral cloning. In *Conference on Robot Learning (CoRL)*, 2021.

Michael Fuest, Pingchuan Ma, Ming Gui, Johannes Schusterbauer, Vincent Tao Hu, and Bjorn Ommer. Diffusion models and representation learning: A survey. *arXiv preprint arXiv:2407.00783*, 2024.

Divyansh Garg, Shuvam Chakraborty, Chris Cundy, Jiaming Song, and Stefano Ermon. Iq-learn: Inverse soft-q learning for imitation. In *Advances in Neural Information Processing Systems (NeurIPS)*, 2021.

David Ha and Jürgen Schmidhuber. World models. *arXiv preprint arXiv:1803.10122*, 2018.

Josiah Hanna and Peter Stone. Grounded action transformation for robot learning in simulation. In *Proceedings of the AAAI Conference on Artificial Intelligence*, volume 31, 2017.

Philippe Hansen-Estruch, Ilya Kostrikov, Michael Janner, Jakub Grudzien Kuba, and Sergey Levine. Idql: Implicit q-learning as an actor-critic method with diffusion policies. *arXiv preprint arXiv:2304.10573*, 2023.

Jonathan Ho and Stefano Ermon. Generative adversarial imitation learning. *Advances in neural information processing systems*, 29, 2016.

Jonathan Ho, Ajay Jain, and Pieter Abbeel. Denoising diffusion probabilistic models. *Advances in neural information processing systems*, 33:6840–6851, 2020.

Tao Huang, Guangqi Jiang, Yanjie Ze, and Huazhe Xu. Diffusion reward: Learning rewards via conditional video diffusion. In *European Conference on Computer Vision*, pages 478–495. Springer, 2024.

Michael Janner, Yilun Du, Joshua B Tenenbaum, and Sergey Levine. Planning with diffusion for flexible behavior synthesis. *arXiv preprint arXiv:2205.09991*, 2022.

Rahul Kidambi, Aravind Rajeswaran, Praneeth Netrapalli, and Thorsten Joachims. Morel: Model-based offline reinforcement learning. *Advances in neural information processing systems*, 33:21810–21823, 2020.

Geon-Hyeong Kim, Seokin Seo, Jongmin Lee, Wonseok Jeon, HyeongJoo Hwang, Hongseok Yang, and Kee-Eung Kim. Demodice: Offline imitation learning with supplementary imperfect demonstrations. In *International Conference on Learning Representations*, 2021.

Geon-Hyeong Kim, Jongmin Lee, Youngsoo Jang, Hongseok Yang, and Kee-Eung Kim. Lobsdice: Offline learning from observation via stationary distribution correction estimation. *Advances in Neural Information Processing Systems*, 35:8252–8264, 2022.

- Ilya Kostrikov, Ashvin Nair, and Sergey Levine. Imitation learning via off-policy distribution matching. In *International Conference on Learning Representations (ICLR)*, 2020.
- Ilya Kostrikov, Ashvin Nair, and Sergey Levine. Offline reinforcement learning with implicit q-learning. *arXiv preprint arXiv:2110.06169*, 2021.
- Michael Laskin, Aravind Srinivas, and Pieter Abbeel. Curl: Contrastive unsupervised representations for reinforcement learning. In *International Conference on Machine Learning*, pages 5639–5650. PMLR, 2020.
- Michael Laskin, Denis Yarats, Hao Liu, Kimin Lee, Albert Zhan, Kevin Lu, Catherine Cang, Lerrel Pinto, and Pieter Abbeel. Urlb: Unsupervised reinforcement learning benchmark. *arXiv preprint arXiv:2110.15191*, 2021.
- Sergey Levine, Aviral Kumar, George Tucker, and Justin Fu. Offline reinforcement learning: Tutorial, review, and perspectives on open problems. *arXiv preprint arXiv:2005.01643*, 2020.
- Hao Liu and Pieter Abbeel. Behavior from the void: Unsupervised active pre-training. In *Advances in Neural Information Processing Systems*, volume 34, 2021.
- YuXuan Liu, Abhishek Gupta, Pieter Abbeel, and Sergey Levine. Imitation from observation: Learning to imitate behaviors from raw video via context translation. In *2018 IEEE international conference on robotics and automation (ICRA)*, pages 1118–1125. IEEE, 2018.
- Yecheng Ma, Andrew Shen, Dinesh Jayaraman, and Osbert Bastani. Versatile offline imitation from observations and examples via regularized state-occupancy matching. In *International Conference on Machine Learning*, pages 14639–14663. PMLR, 2022.
- Ajay Mandlekar, Danfei Xu, Josiah Wong, Soroush Nasiriany, Chen Wang, Rohun Kulkarni, Li Fei-Fei, Silvio Savarese, Yuke Zhu, and Roberto Martín-Martín. What matters in learning from offline human demonstrations for robot manipulation. In *Conference on Robot Learning*, pages 1678–1690. PMLR, 2022.
- Dean Pomerleau. Alvinn: An autonomous land vehicle in a neural network. In *Advances in Neural Information Processing Systems (NeurIPS)*, 1989.
- Olaf Ronneberger, Philipp Fischer, and Thomas Brox. U-net: Convolutional networks for biomedical image segmentation. In *International Conference on Medical image computing and computer-assisted intervention*, pages 234–241. Springer, 2015.
- Stéphane Ross, Geoffrey Gordon, and Drew Bagnell. A reduction of imitation learning and structured prediction to no-regret online learning. In *Proceedings of the fourteenth international conference on artificial intelligence and statistics*, pages 627–635. JMLR Workshop and Conference Proceedings, 2011.

- Nur Muhammad Shafiullah, Zichen Cui, Ariuntuya A Altanzaya, and Lerrel Pinto. Behavior transformers: Cloning k modes with one stone. In *Advances in Neural Information Processing Systems (NeurIPS)*, 2022.
- Harshit Sikchi, Caleb Chuck, Amy Zhang, and Scott Niekum. A dual approach to imitation learning from observations with offline datasets. *arXiv preprint arXiv:2406.08805*, 2024.
- Shashank Singh, Neeraj Misra, Vladimir Hnizdo, Adam Fedorowicz, and Eugene Demchuk. Nearest-neighbor estimates of entropy. *American Journal of Mathematical and Management Sciences*, 23 (3-4):301–321, 2003.
- Bradly C Stadie, Pieter Abbeel, and Ilya Sutskever. Third person imitation learning. In *International Conference on Learning Representations*, 2017.
- Denis Tarasov, Vladislav Kurenkov, Alexander Nikulin, and Sergey Kolesnikov. Revisiting the minimalist approach to offline reinforcement learning. *Advances in Neural Information Processing Systems*, 36: 11592–11620, 2023.
- Yonglong Tian, Lijie Fan, Phillip Isola, Huiwen Chang, and Dilip Krishnan. Stablerep: Synthetic images from text-to-image models make strong visual representation learners. *Advances in Neural Information Processing Systems*, 36:48382–48402, 2023.
- Faraz Torabi, Garrett Warnell, and Peter Stone. Behavioral cloning from observation. *arXiv preprint arXiv:1805.01954*, 2018.
- Qi Wang, Mian Wu, Yuyang Zhang, Mingqi Yuan, Wenyao Zhang, Haoxiang You, Yunbo Wang, Xin Jin, Xiaokang Yang, and Wenjun Zeng. Goal-driven reward by video diffusion models for reinforcement learning. *arXiv preprint arXiv:2512.00961*, 2025.
- Zhendong Wang, Jonathan J Hunt, and Mingyuan Zhou. Diffusion policies as an expressive policy class for offline reinforcement learning. In *The Eleventh International Conference on Learning Representations*.
- Kai Yan, Alexander C Zhang, and Yunzhu Li. Offline imitation from observation via primal wasserstein state occupancy matching. In *International Conference on Machine Learning (ICML)*, 2024.
- Xingyi Yang and Xinchao Wang. Diffusion model as representation learner. In *Proceedings of the IEEE/CVF International Conference on Computer Vision*, pages 18938–18949, 2023.
- Amy Zhang, Rowan McAllister, Roberto Calandra, Yarin Gal, and Sergey Levine. Learning invariant representations for reinforcement learning without reconstruction. In *International Conference on Learning Representations*, 2020.

Konrad Zolna, Alexander Novikov, Ksenia Konyushkova, Caglar Gulcehre, Ziyu Wang, Yusuf Aytar, Misha Denil, Nando De Freitas, and Scott Reed. Offline learning from demonstrations and unlabeled experience. *arXiv preprint arXiv:2011.13885*, 2020.

A Hyperparameters and Implementation Details

A.1 Hyperparameters

We list the hyperparameters used for the diffuser, including details of the U-Net architecture, as well as those for TGE reward estimation in Table 2. We also report the hyperparameters for the downstream offline RL backbones, IQL and ReBRAC, in Tables 3 and 4, respectively. For all baseline methods, we strictly follow the original implementations and hyperparameter settings reported in their respective papers.

Table 2: **Hyperparameter settings for TGE.** The hyperparameters below are used to train the trajectory-level generative planner and estimate the rewards.

Hyperparameter	Value
<i>Reward Estimation</i>	
Kernel type	Laplacian
Kernel temperature (τ)	1.0
Number of nearest neighbors (m)	10
<i>Diffuser Architecture</i>	
Diffuser horizon (H)	32
Channel multipliers	(1, 2, 4, 8)
Diffusion steps	20
Embedding dimension	64
Learning rate	2e-4
Batch size	32
EMA decay	0.995
Scheduler	DDPMsScheduler

Table 3: **Hyperparameter Settings for IQL.**

Hyperparameter	Value
<i>Optimizer</i>	
Optimizer	AdamW
Actor Learning rate	$3e - 4$
Critic Learning rate	$3e - 4$
Value Function Learning rate	$3e - 4$
Batch size	1024
<i>Algorithm Specifics</i>	
Discount factor (γ)	0.99
Target smoothing (τ_{target})	0.005
Expectile (τ)	0.8
Inverse Temperature (β)	0.5
Dropout rate	0 (Mujoco) / 0.1(Adriot)

Table 4: **Hyperparameter Settings for ReBRAC.** For the actor BC coefficient, values $\{1.0, 0.5, 0.1, 10.0\}$ are used for $\{\text{Others}, \text{Hopper-random}, \text{HalfCheetah-random}, \text{Adroit-Cloned}\}$, respectively. For the critic BC coefficient, values $\{1.0, 0.5, 0.0\}$ correspond to $\{\text{Others}, \text{HalfCheetah-random}, \text{Adroit-Cloned}\}$, respectively.

Hyperparameter	Value
<i>Optimizer & Architecture</i>	
Optimizer	AdamW
Actor Learning rate	$3e - 4$
Critic Learning rate	$3e - 4$
Weight decay	$1e - 4$
Batch size	1024
Hidden layers	3
Hidden dimension	256
Layer normalization	True (Mujoco) / False (Adriot)
<i>Algorithm Specifics</i>	
Discount factor (γ)	0.99
Target smoothing (τ_{target})	0.005
Policy update frequency	2
Policy noise (σ)	0.2
Noise clip	0.5
Actor BC coefficient (β_{actor})	1.0, 0.5, 0.1, 10.0
Critic BC coefficient (β_{critic})	1.0, 0.5, 0.0

A.2 Implementation Details

We implement the TGE reward as the log-likelihood of an m -nearest-neighbor kernel density estimator (KDE) defined in the trajectory-level latent embedding space. All embeddings are first normalized to the unit hypersphere ($z \leftarrow z/\|z\|_2$). Distances are computed using Euclidean distance on the sphere, which is monotonic with cosine distance ($\|z_i - z_j\|_2 = \sqrt{2 - 2 \cos \theta}$).

For each offline transition, we retrieve its m nearest expert neighbors in the embedding space (with $m=10$ by default) and compute kernel values using a Laplacian kernel, $f = \exp(-d/\tau)$. We adopt this linear log-decay rather than a Gaussian kernel with quadratic decay, as the latter tends to produce overly sparse reward signals in high-dimensional embedding spaces and weak supervision for suboptimal data. The neighbor kernel values are then aggregated using a Log-Sum-Exp operation to produce the final reward, which can be interpreted as a robust soft minimum distance to the expert support.

Finally, we train offline policies using IQL and ReBRAC as drop-in backbones, relying solely on \mathcal{D}_μ and the learned TGE reward, without any online interaction.

B Details of the Mixture Strategy for the Suboptimal Dataset

We provide a detailed breakdown of the data mixture strategy used to construct the suboptimal dataset \mathcal{D}_μ . Following established protocols in offline imitation learning from observations introduced in [Ma et al., 2022, Sikchi et al., 2024], we construct \mathcal{D}_μ by combining a large corpus of suboptimal transitions with a limited number of expert trajectories. Table 5 summarizes the detailed composition for all suboptimal datasets.

Table 5: **Dataset Mixture Details.** We summarize the data mixture strategies for the suboptimal datasets \mathcal{D}_μ used across different experimental settings.

Dataset Name	Suboptimal Data	Expert Trajectories	Episode Length
<i>Locomotion Tasks</i>			
Random + Expert	1e6 transitions	200	1000
Medium + Expert	1e6 transitions	200	1000
Random + Few-Expert	1e6 transitions	30	1000
Medium + Few-Expert	1e6 transitions	30	1000
Medium	1e6 transitions	0	1000
<i>Adroit Tasks</i>			
Pen (Cloned + Expert)	5e5 transitions	30	100
Pen (Human + Expert)	5e3 transitions	30	100
Door (Cloned + Expert)	1e6 transitions	30	200
Door (Human + Expert)	6.7e3 transitions	30	200
Hammer (Cloned + Expert)	1e6 transitions	30	200
Hammer (Human + Expert)	1.1e4 transitions	30	200

C Additional Ablation Studies

C.1 Kernel Temperature

We investigate the sensitivity of our framework to the kernel temperature τ , which regulates the decay rate of the Laplacian kernel and determines the sharpness of the reward signal in the latent space. Table 6 reports the normalized scores on `Walker2d-medium` and `Hopper-random` across a wide range of values $\tau \in \{0.1, 0.5, 1.0, 2.0, 5.0\}$.

As shown in the results, TGE demonstrates remarkable robustness to this hyperparameter. Despite varying τ by an order of magnitude, the performance fluctuations remain minimal. These findings confirm that the proposed trajectory-level embedding provides a well-structured metric space where the relative proximity of trajectories is preserved. Consequently, precise task-specific tuning of τ is

unnecessary, and we adopt $\tau = 1.0$ as the default to balance signal discriminativeness and smoothness.

Table 6: **Ablation on Kernel Temperature (τ).** We compare normalized scores across varying temperatures. The method shows robust performance for $\tau \in [0.1, 5.0]$.

Environment	Kernel Temperature (τ)				
	$\tau = 0.1$	$\tau = 0.5$	$\tau = 1.0$ (Default)	$\tau = 2.0$	$\tau = 5.0$
Walker2d-medium	106.60 \pm 2.79	105.98 \pm 1.20	105.79 \pm 2.07	105.31 \pm 3.47	103.69 \pm 7.03
Hopper-random	107.77 \pm 2.50	107.88 \pm 1.70	109.19 \pm 0.41	108.23 \pm 3.17	106.60 \pm 2.79

C.2 Number of Nearest Neighbors

We evaluate the influence of the number of nearest neighbors m on the final performance by changing the value across $m \in \{1, 3, 5, 10, 20\}$. As shown in Table 7, the empirical results demonstrate that our method is remarkably insensitive to the choice of m . Across all tested values, the normalized scores remain highly consistent, with fluctuations largely falling within the standard deviation. This stability indicates that the learned trajectory embeddings are sufficiently discriminative to provide high-quality reward signals even with a small m , while remaining robust to over-smoothing at larger m . Given this robustness, we adopt $m = 10$ as a fixed default for all experiments.

Table 7: **Ablation on Number of Nearest Neighbors (m).** We evaluate the impact of hyperparameter m on the performance over Walker2d medium and Hopper random settings.

Environment	Number of Nearest Neighbors (m)				
	$m = 1$	$m = 3$	$m = 5$	$m = 10$ (Default)	$m = 20$
Walker2d-medium-v2	104.67 \pm 5.97	102.78 \pm 5.06	106.62 \pm 1.16	105.79 \pm 2.07	102.31 \pm 5.01
Hopper-random-v2	107.69 \pm 2.07	106.07 \pm 4.54	103.06 \pm 6.82	110.08 \pm 1.51	105.05 \pm 5.88

D Training Dynamics Visualizations

We provide the training curves of TGE combined with IQL and ReBRAC as downstream offline RL methods across different environments to demonstrate the training stability of our proposed method. Figure 5 and Figure 6 visualize the normalized D4RL score (y-axis) over training steps (x-axis) for the IQL and ReBRAC backbones, respectively.

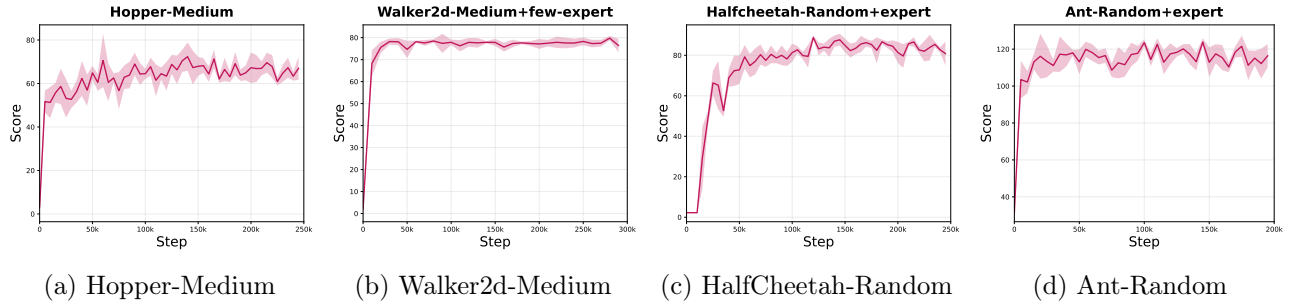


Figure 5: **Training Dynamics of TGE + IQL.** The curves display the mean normalized score and standard deviation (shaded region). TGE combined with IQL shows stable policy improvement, confirming that our geometric reward signal enables robust learning across different offline RL methods.

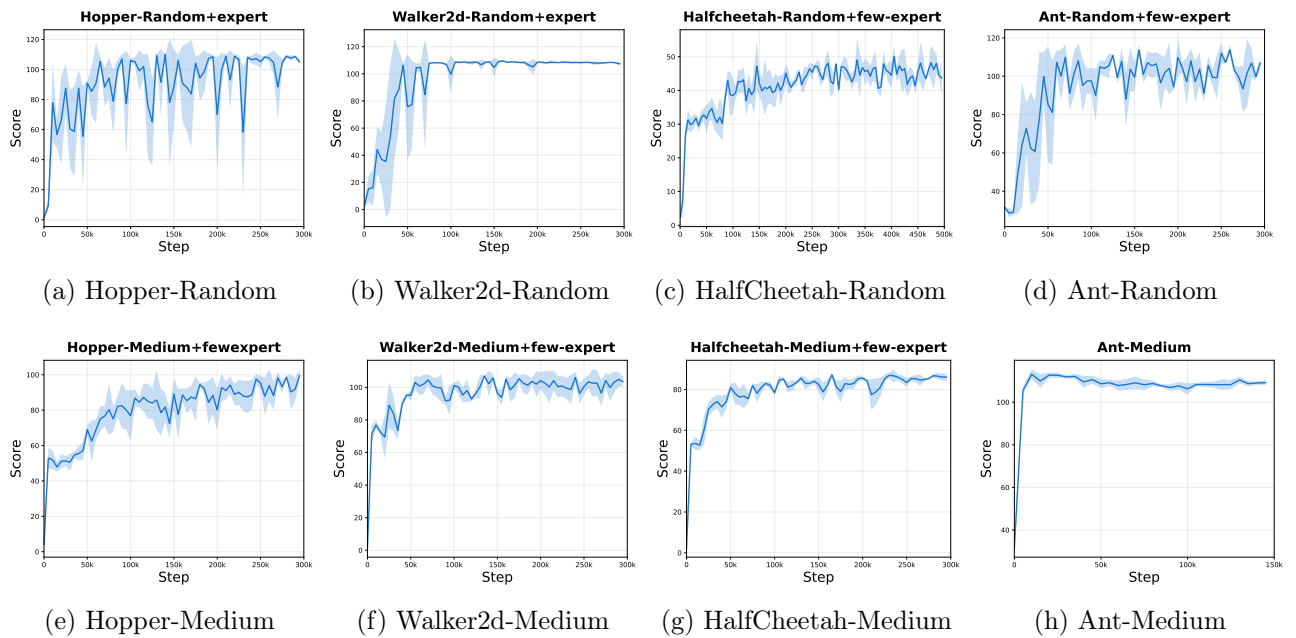


Figure 6: **Training Dynamics of TGE + ReBRAC.** The curves display the mean normalized score and standard deviation (shaded region). Similarly, the results demonstrate that the agent achieves rapid convergence to expert-level performance and maintains asymptotic stability, effectively robust to the noise in suboptimal datasets.